Dynamical and statistical properties of high-temperature self-propagating fronts: An experimental study

A. S. Rogachev*
Institute of Structural Macrokinetics and Materials Science, Russian Academy of Sciences, 142432 Chernogolovka, Russia

F. Baras†
Institut Carnot de Bourgogne, UMR 5209 CNRS-Université de Bourgogne, 21078 Dijon, France

(Received 5 September 2008; published 19 February 2009)

We present a detailed experimental study of high-temperature self-propagating fronts using image processing techniques. The intrinsic features of the wave propagation are investigated as a function of the combustion temperature T_C for a model system made of titanium and silicon powders. Different front behavior is realized by changing the molar ratio x of the mixture Ti+xSi. Outside the range $x=[0.3,1.5]$, no thermal front is propagating while inside, three regimes are observed: steady-state combustion which is characterized by a flat front propagating at constant velocity and two unsteady regimes. The combustion temperature (or the corresponding ratio x) is thus playing the role of bifurcation parameter leading from stationary state to complex behavior. In the titanium-rich mixture, the position of the front oscillates and hot spots propagate along the external border of the sample. At lower amounts of Ti, localized bright regions appear randomly and deform the front profile. The associated dynamical behavior is a relay-race mechanism which becomes more pronounced close to the combustion limit. Methods are developed to characterize the structural and dynamical properties of thermal waves near instabilities, with a special emphasis on the statistical aspects. It is clearly demonstrated that the mesoscopic scale phenomena interfere significantly with the macroscopic behavior. The experiments reveal front behaviors that cannot be described using the usual macroscopic theories.

DOI: 10.1103/PhysRevE.79.026214 PACS number(s): 05.45.−a, 05.65.+b, 82.20.−w

I. INTRODUCTION

Nonlinear phenomena are ubiquitous from physical to life science [1]. Under nonequilibrium conditions, they are associated with the development of complex behaviors such as multiple states, abrupt transitions, periodic or chaotic oscillations, waves, and spatial patterns [2–4]. These instabilities are usually predicted in the framework of the macroscopic description offered by the phenomenological equations. In some cases, it nevertheless becomes crucial to develop a statistical approach for the complex transitions and instability phenomena [5]. The statistical study of instabilities allows one to identify situations in which the microscopic dynamics interferes significantly with processes at the macroscopic level. In such situations, the very possibility of a clear-cut separation between macro- and micro-behaviors becomes questionable. For instance, when reactive and transport processes are taking place in low-dimensional supports, the intrusion of the microscopic dynamics into the collective behavior becomes especially striking and leads to the breakdown of the usual mean-field description [6,7]. Another significant case is given by transient phenomena associated with explosive behavior. It appears that the sensitivity of explosive systems to perturbations of various origin causes new effects which have no analog in the macroscopic rate equations, such as the randomness of the ignition time [8–10]. In this paper, we present experimental results on the emergence of instabilities in highly exothermic systems and we develop the corresponding statistical analysis based on image-processing techniques. By using a multiscale description, we will show to what extent the mesoscopic scale phenomena interfere with the macroscopic behavior.

The most significant aspect of exothermic reactions is thermal feedback. At the macroscopic level, it is manifested through the strongly nonlinear dependence of the Arrhenius factor on temperature and can lead to abrupt transitions. Depending on initial and boundary conditions, we may observe abrupt phenomena in timelike explosions or steep propagating waves associated with the exothermic reaction. In this paper, we will focus more specifically on the latter situation.

From the experimental point of view, we study the propagation of reaction waves in a mixture of solid powders (particle size 40–150 μm) compressed into small samples (e.g., cylinders of 1 to 2 cm long with a diameter of about 1 cm). In many situations, the reaction between the solid reagents say A and B can be approximated by a dominant one-step irreversible scheme of the form

$$A + B \rightarrow C + \text{heat}. \tag{1}$$

After the initiation by heating the sample at one end, a highly exothermic combustion starts locally. The resulting heat released propagates to the contiguous regions, initiating in turn new seats of combustion. This mechanism leads quite rapidly to the formation of a stable reaction front that propagates through the system with a practically constant velocity, at least in the steady combustion regime. Indeed, front oscillations about the average speed or even more complex phenomena such as chaos and spinning waves may also occur [11–13]. The propagation of the thermal wave is associated

*rogachev@ism.ac.ru
†fbaras@u-bourgogne.fr

with the formation of compound C because the heat released by the reaction supplies the energy for the synthesis. Such a process is usually called combustion synthesis or self-propagation high-temperature synthesis (SHS) (for a general review, see [14,15]). The heating rate due to the exothermic reaction can be quite high (10^3–10^6 K s^{-1}) and the combustion temperature may also reach extremely high values (2300–3500 K). The overall process thus takes place under very strong nonequilibrium conditions in short reaction times (on the order of seconds). The main feature of this system relies on the heterogeneous nature of the support which introduces a natural mesoscopic scale associated with the size of the particles. Despite extensive investigations, the mechanisms of reaction propagation in heterogeneous media are not completely understood.

During the last decade, a new investigation method has been developed to analyze the structural properties of the thermal front associated with fast chemical reactions taking place in heterogeneous media [16,17]. This allows one to observe *in situ* rapid processes (up to 10^{-4} s) occurring at the microscopic level (up to 1 μm). Such microscopic studies of gasless combustion have shown that at small time scales the behavior of self-propagating high-temperature reaction waves can become complex [18,19]. Accordingly to the structure of the front, two modes of propagation have been identified: the quasihomogeneous reaction wave (QRW) which corresponds to a planar steady state of propagation and the scintillating reaction wave (SRW) which cannot be predicted by the usual macroscopic approach. The later is characterized by short hot spots which randomly arise in the vicinity of the front and induce the global propagation of the front. Most studies are aimed at establishing a correlation between the thermal heterogeneity of the reaction front and the microstructure of the initial powder mixture. The influence of parameters such as density and porosity of the initial medium has been investigated as well as the influence of reactant particle size on the propagation properties [20]. In this work, we have studied the dynamical and structural properties of combustion synthesis fronts in the vicinity of steady-state limits and instabilities. For this purpose, we have developed a detailed statistical approach based on "*in situ*" characterization to understand the influence of mesoscopic processes on macroscopic instabilities.

The paper is organized as follows. The macroscopic modeling of thermal waves in solid systems, as well as a brief description of the instabilities associated with it, is presented in Sec. II. The experimental procedure is explained in Sec. III; we present the specific system we have studied, the experimental set up, and the imaging. Section IV contains the detailed review of our results that are discussed in Sec. V. The main conclusions are summarized in Sec. VI.

II. OVERVIEW OF THEORY

The traditional description of solid-phase combustion is based on the heat-transfer equation combined with a source term representing an exothermic reaction [22]. In experimental situations, the reacting sample usually has cylindrical geometry and in many circumstances the variation of the temperature field T along the lateral direction is small and can be ignored. Upon neglecting lateral heat losses, the one-dimensional macroscopic equations that describe the evolution of the temperature of such a system read

$$\rho C_p \frac{\partial T}{\partial t} = \lambda \frac{\partial^2 T}{\partial x^2} + \rho Q \phi(T,\eta) \tag{2a}$$

$$\frac{\partial \eta}{\partial t} = \phi(T,\eta), \quad 0 \leqslant \eta \leqslant 1, \tag{2b}$$

where ρ is the mass density, C_p the specific heat at constant pressure, λ the thermal conductivity, Q the heat of reaction, η the "degree of conversion" whose time evolution is defined in Eq. (2b), and ϕ the reaction rate which is assumed to obey the Arrhenius law. For a first-order reaction, the explicit form of ϕ reads

$$\phi(T,\eta) = k_0(1-\eta)\exp(-E/RT), \tag{3}$$

where E is the activation energy and k_0 is a constant. Note that there exist more complicated forms for ϕ that are used in order to take into account some specific aspects of the reactive processes, such as higher order reactions, the porosity of the media, etc. [23]. In this paper we shall restrict ourselves to the simple form (3) and assume that all the parameters (heat conductivity coefficients, heat capacity, etc.) remain constant during the process.

The exothermic reaction is commonly initiated by heating one end of the cylinder. From a theoretical point of view, this is equivalent to setting the temperature at one of the boundaries, say $x=0$, to a specific value T_i, and the rest of the sample at the ambient temperature T_0 at $t=0$. The initial and boundary conditions thus read

$$T(x,0) = T_0, \quad 0 < x \leqslant L,$$

$$T(0,t) = T_i; \quad \lambda \left.\frac{\partial T(x,t)}{\partial x}\right|_{x=L} = 0, \tag{4}$$

where L is the length of the sample. Note that more realistic boundary conditions may be adopted at $x=L$, which may, for example, include the radiative energy transfer as well. However, our main purpose here is to analyze the behavior of the temperature in the bulk (near the middle of the system), which proves to be quite insensitive to the adopted boundary conditions.

It is instructive to consider first the case of a perfectly homogeneous and adiabatically isolated system. Dropping the heat transfer term in Eqs. (2), one can easily check that the quantity $C=T(t)-\eta(t)Q/C_p$ remains constant in the course of time. Since initially $\eta=0$, one has $C=T_0$. On the other hand, the temperature reaches its maximum value, T_c, once the reactive process has been completed, i.e., $\eta=1$, so that $C=T_c-Q/C_p$. It follows that

$$T_c = \frac{Q}{C_p} + T_0, \tag{5}$$

T_c is usually called "adiabatic temperature" or "combustion temperature." It represents an upper bound for the tempera-

ture in real systems where lateral cooling and heat transport processes are both present.

The set of equations (2) have been the subject of extensive analysis, both theoretically and numerically. Basically, once the reaction is initiated, one observes the formation of a heat front that, after a short delay, starts to propagate with a constant speed up to the vicinity of the outer boundary, $x=L$. However, under some particular circumstances, this "stationary regime" may become unstable.

From a theoretical point of view, the stability of the stationary regime can be characterized by two dimensionless parameters, β and γ, which are sometimes called, respectively, the Arrhenius and the Todes parameters. They are defined as

$$\beta = \frac{RT_c}{E}, \tag{6a}$$

$$\gamma = \frac{RT_c^2}{E(T_c - T_0)}. \tag{6b}$$

In particular, it has been shown analytically that Eqs. (2) admit a stable propagating wave solution with a constant speed as long as the following inequality holds [11,24]:

$$\gamma > \sqrt{5} - 2 \approx 0.236. \tag{7}$$

If the value of γ is below this threshold, the system first undergoes a Hopf bifurcation, resulting in a front that moves with a pulsating speed. As γ decreases further, higher order bifurcations gradually occur, leading to a succession of period doubling transitions, that may eventually end up in a chaotic regime.

The criterion (7) was derived analytically and is only applicable to one-dimensional systems, where the main relevant variable is the speed of the front. A more precise stability criterion was obtained with the help of extensive computer simulations [25]. In particular, it has been shown that the overall stability of the front can be characterized by a single parameter α_{st}, defined as

$$\alpha_{st} = 9.1\gamma - 2.5\beta. \tag{8}$$

For $\alpha_{st} > 1$, the heat front propagates with a stable plane shape at constant speed. As soon as $\alpha_{st} < 1$, the plane shape of the heat front becomes unstable, leading to the formation of a variety of exotic complex waves. This regime is called spin combustion and is considered as a two-dimensional disturbance of the flat front. In a cylindrical geometry, Maksimov *et al.* [26] suggest that there is steplike distortion of the front along the radius, which rotates like a beam of light from a lighthouse. Ivleva and Merzhanov [13,27,28], proposed rather more complex shapes which can be associated with a spiral-helix motion of a localized combustion center occurring along the lateral surface of the cylinder, very much like a rotating wavy bowl. In any case, the rotation is smooth with a constant angular speed.

The traditional way of exploring the stability properties of the system is to start with a stable front propagation regime and lower α_{st} gradually. This can be done either by increasing the value of the activation energy E or lowering that of the combustion temperature T_c. From an experimental point of view, the latter proves to be much easier to achieve than the former. There are three ways to lower T_c: decrease the initial temperature T_0, decrease the reaction heat released Q by adding inert components to the sample, and, finally, modify its initial composition. In this experimental study, we have chosen the last one mainly because it is the easiest way to monitor the initial state of the system.

III. EXPERIMENTAL PROCEDURE

We consider a solid phase reaction involving a mixture of silicon and titanium powders, known as "Ti-Si system." The reactive process is commonly represented in the form Ti $+x$Si, where the stoichiometric coefficient x can be considered as the bifurcation parameter [36]. For instance, it is known that combustion occurs for values of x ranging from 0.3 to 2.4 [29,30]. An oscillatory regime has also been observed at the higher end of this range [29], while spin combustion was reported at $x \approx 1$ for coarse Ti powder [30]. A nice characteristic of the Ti-Si system is that the amount of gas released during the reaction turns out to be relatively small, making the experimental visualization of the front quite accurate. It is therefore well-suited for video recording that allows a detailed analysis of the development of front instabilities near the combustion limits. Since it is relatively easy to visualize the propagating reaction front, this system has already been used for the study of the reaction front's microstructures, as a function of the size of the particles and the porosity of the sample [20]. In what follows, we explain the experimental procedure and the image analysis.

In our experimental set up, we use typical commercial grade powders with the following characteristics: Ti, 100 mesh Ð 010383 Alfa Aesas, and Si, 325 mesh Ð ERAG S-1053. The size of Ti particles is about 150 μm whereas that of Si particles is less than 50 μm. For both powders, the impurity is less than 1%. They are dry-mixed in a wobbling mixer (Dyno1000), without milling bodies, to avoid any change of the particle sizes, and then they are pressed uniaxially in a cylindrical die. The typical dimensions of the sample are about 13 mm in diam and 12 mm in height. The samples have a porosity of 40%–45%. With a hydraulic press, it is difficult to prepare larger samples without introducing a porosity gradient. The composition of the mixture of powders Ti$+x$Si, characterized by the stoichiometric coefficient x, ranges from $x=0.3$ to 2. We keep a fixed sample porosity and dimensions in all our experiments. This can be done by controlling the mass of the sample for each value of the composition parameter x.

A schematic diagram of the experimental set up is shown in Fig. 1. The sample is put in the reaction chamber, which is filled with an inert gas. A tungsten coil connected to a power supply is heated to initiate the reaction in a thin pellet made with the most exothermic composition ($x=0.6$); the thin pellet is in contact with the sample. The heat released by the pellet initiates in turn the reaction in the sample. This experimental procedure ensures the same ignition conditions for all the experiments and ensures uniform heating of the sample's cross section.

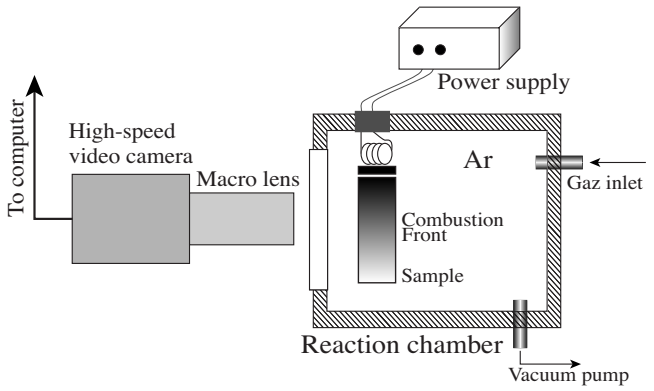

FIG. 1. Schematic diagram of the combustion chamber and the digital high-speed video recording technique.

Front propagation is recorded through a window using a high-speed video camera (Kodak motion corder analyzer SR-500) in macro mode and equipped with appropriate filters (red, blue, or both). The recording rate is set to 250 frames/s, with a sensor input of 512×480 pixels. Each pixel has therefore a spatiotemporal resolution of 40 μm and 4 ms, respectively. One pixel corresponds approximately to the size of a silicon particle. Recording of the propagating front is stopped manually by the operator when the combustion looks complete. In this way, we get a set of digital images that correspond to the evolution of the propagation front in the sample. The images are imported into a computer and analyzed using MatLab.

Through image analysis, we study the location of the front, its shape, and the propagation characteristics. The pixel intensity matrix at time t is represented by $z(i,j,t)$ in which i is the row (horizontal line in Fig. 2) and j the column. To locate the position of the front, we use the following method.

(1) For each row, we compute the mean value of the pixel intensity

$$z_{\mathrm{m}}(i,t) = \frac{1}{N_C} \sum_{j=1}^{N_C} z(i,j,t),$$

where N_C represents the number of columns.

(2) We next define a given threshold intensity z^*, typically of the order of half of the maximum intensity. Going from top to bottom (see Fig. 2), the mean position of the front $Y_{f,m}(t)$ corresponds then to the value of the row index for which the inequality $z_{\mathrm{m}}(i,t) < z^*$ occurs for the first time.

(3) The front shape $Y_f(j,t)$ is obtained using a similar rule $z(i,j,t) < z^*$. If this value is out of range, we set $Y_f(j,t) = Y_{f,m}(t) \pm \delta$, where δ is chosen approximative as the variance of the position. This allows one to eliminate the spurious dark and bright spots not directly associated with the front. Such spurious bright spots appear due to the presence of burning dusts, isolated jets of ignition, or cavities in the sample.

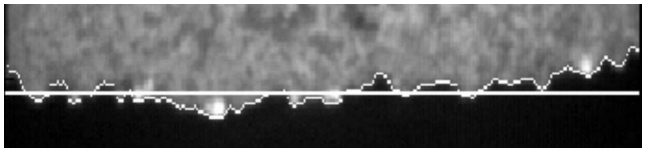

FIG. 2. Image of the instantaneous profile of the front and mean position (white line). The height of the visualization window is about 3 mm.

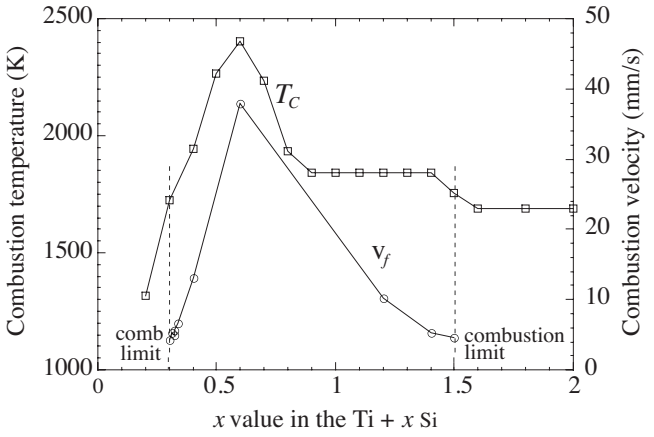

FIG. 3. Combustion temperature T_C (squares: scale in K, on the left) and front velocity v_f (bullets: scale in mm/s, on the right) as a function of the stoichiometry x of the initial sample.

In Fig. 2, the front location (in white) is plotted directly on the image. The straight line corresponds to the mean position of the front. The mean position as a function of time gives directly an estimation of the propagation velocity.

IV. RESULTS

We first evaluate the macroscopic propagation velocity v from the mean position of the front $Y_{f,m}$. The dependence of v_f on the stoichiometric coefficient is shown in Fig. 3, together with the predetermined adiabatic combustion temperature T_c. The maximum velocity (about 38 mm/s) coincides with the highest value of T_c for $x=0.6$. This is expected from the phase diagram since the more exothermic alloy corresponds precisely to the synthesis $5\mathrm{Ti}+3\mathrm{Si} \rightarrow \mathrm{Si}_3\mathrm{Ti}_5$. The formation of this alloy releases the largest amount of heat which contributes to an increase of the corresponding combustion temperature. The front velocity decreases in the range $x=1-1.4$ although the adiabatic temperature is constant. This indicates that the Zeldovich model which predicts a dependence of velocity v_f on the temperature T_c [$\ln(v_f) \approx -E/RT_c$, where E is the activation energy] is not always valid in the case of a solid flame as shown in [21]. In heterogeneous mixtures such as $\mathrm{Ti}+x\mathrm{Si}$, the adiabatic temperature is not the only governing parameter for propagation velocity where combustion is accompanied by complex microstructural and phase transformations.

Outside the range $x=[0.3,1.5]$, no propagating combustion front is observed. The existence of combustion limits is well-known in the literature. Our results for the concentration limits in excess of Ti and Si are in good agreement with previous studies [27,28]. Quantitative differences may follow as the consequence of some microstructure properties, like, for instance, the particle size of the powder.

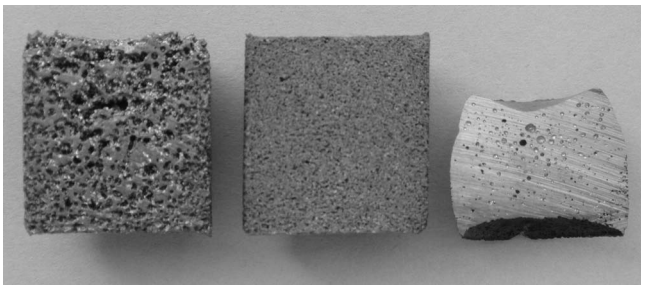

FIG. 4. Cross sections of the synthesized samples for three representative compositions: Si excess $x=1.4$ (left), $x=0.6$ (center), and Ti excess with $x=0.322$ (right).

It is interesting to compare the melting temperature of the two reactants $T_m(\mathrm{Ti})=1933$ K and $T_m(\mathrm{Si})=1683$ K with the combustion temperature. We see that $T_C(x=0.6)$ is higher than both values. In the range $x\in[0.3,0.4]$ (excess of titanium), the combustion temperature is very close to the Si melting temperature, while for $x>1.2$ (excess of silicon), we have $T_m(\mathrm{Si})<T_C<T_m(\mathrm{Ti})$. These observations clearly show that the reaction operates differently for different values of the stoichiometric ratio x, ranging from nearly solid/solid reaction (excess of Ti) to solid/liquid (excess of Si). Only the ratio $x=0.6$ corresponds to a liquid/liquid synthesis.

The appearance of the final synthesized material is radically different in the three situations of excess of Si ($x=1.4$), Si in stoichiometric amount ($x=0.6$), and excess Ti ($x=0.32$), as shown in Fig. 4. The diameter of the samples is only slightly modified, after the combustion is completed, whereas the height might undergo significant changes. If the Ti is in excess ($x<0.6$), the sample tends to shrink, while in the opposite case ($x>0.6$), the sample may lengthen up to 10%. The video analysis clearly shows that the modifications appear behind the front whose specificities are thus not altered by the modifications of the shape of the samples. On the other hand, the cross sections of the samples reveal a specific structure that depends on the ratio x. For $x=0.6$, the combustion product is characterized by a uniform distribution of fine pores. If Si is in excess ($x>0.6$), we observe large and irregular pores, while in the opposite case (excess of Ti), we get a dense product with a quite small amount of voids. Thanks to the *in situ* characterization of the rapid chemical reaction with the high-speed video camera, we will show how the macrostructure of the final material is directly related to the dynamics of the propagating front. To be able to establish the correlation between macro- and microstructure, we will now present the results concerning the dynamical behavior of the front in the three typical situations.

A. Ti+0.6Si composition

For this composition, the ignition is very rapid with or without an ignition initiating pellet. One-tenth of a second after initiation, a flat front starts to propagate steadily throughout the sample. The overall process with the complete conversion of reactants takes less than 1 s. Figure 5(b) shows successive images of the front every 16 ms (every four frames).

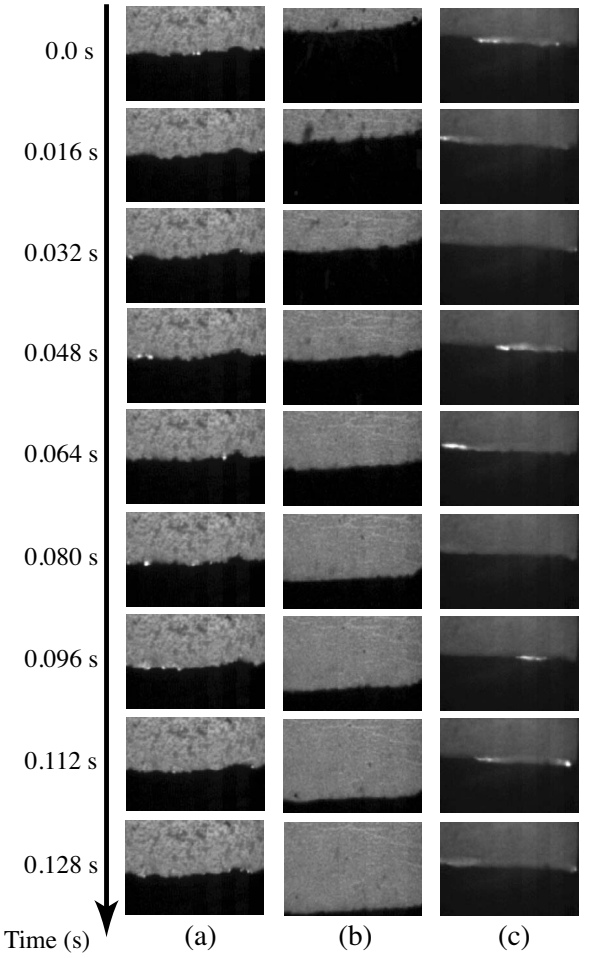

FIG. 5. Snapshots of the front every 16 ms for three representative compositions (a) in excess of Si (Ti+1.4 Si), (b) Ti+0.6 Si, and (c) in excess of Ti (Ti+0.322 Si). The height of the visualization window is about 10 mm.

We clearly observe a steady-state regime with a well-defined velocity. The linear fit of the mean position as a function of time is excellent. All positions along the front are evolving in a similar way with a local velocity close to the mean velocity. The influence of microheterogeneity could eventually be observed at a smaller time scale using a better spatial resolution.

B. Excess of silicon ($x>0.6$)

Images of the front at consecutive times are presented in Fig. 5(a). We note that in an interval of about 100 ms, the front's position changes very little. This is due to the drastic reduction of its propagation speed, as shown by the measurement of the velocity of the mean position which remains possible beside the fact that the front structure is coarse [see Figs. 2 and 5(a)]. One can clearly see bright regions which seem to appear randomly with no apparent correlation between them in the successive pictures.

The snapshot profile presented in Fig. 2 for the composition $x=1.4$ demonstrates the complex structure of the front. We see the appearance of hot spots of different size just

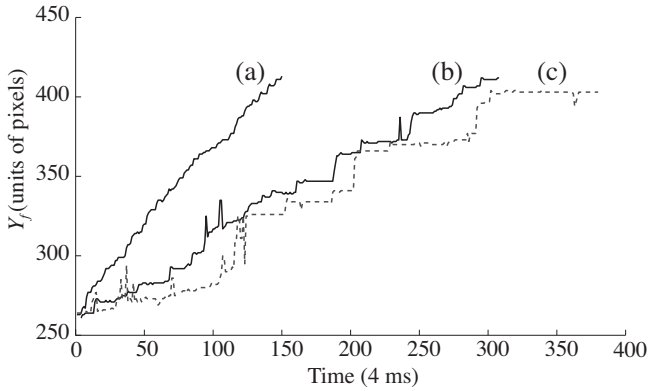

FIG. 6. Illustration of the relay-race mechanism: evolution of the local front position $Y_f(j,t)$ on a given column j in the middle of the sample for different compositions (a) $x=1.2$, (b) $x=1.4$, and (c) $x=1.5$. Position is measured in pixels. Time unit is 4 ms.

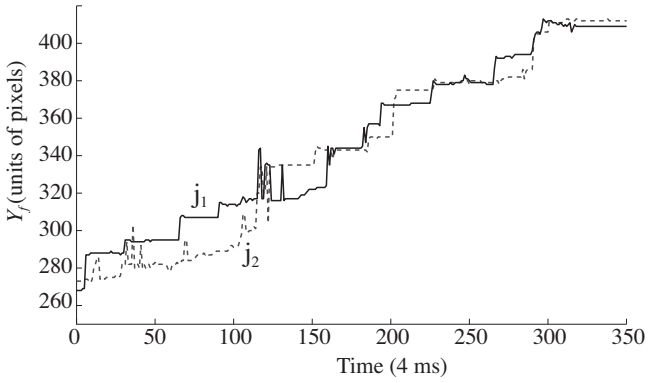

FIG. 8. Evolution of the front position $Y_f(j,t)$ for two adjacent columns $j_1=100$ and $j_2=110$ in the same sample. We observe many crossings between the front positions $Y_f(j_2,t)$ and $Y_f(_1,t)$ during the propagation. This induces a pronounced roughness of the front.

behind the border of the front. Their brightness is associated with the local increase of temperature. The local instantaneous position $Y_f(j,t)$ as a function of time, for j fixed, is plotted in Fig. 6 for values of x ranging from 1.2 to 1.5. For $x=1.2$, the front propagates nearly uniformly and we can measure a well-defined front velocity even locally. For larger x values, it is no longer the case. The velocity along a line is drastically reduced by a factor of 2 when the composition changes from $x=1.2$ to 1.4. Moreover, we see that the front may stop for a while before jumping to its next position. This is particularly evident when there is a large excess of Si. For these stoichiometries, we observe thus a relay-race mechanism which is typical of microheterogeneous supports and has no analog in the macroscopic description.

A representative quantity to characterize this particular behavior is the time delay. We define the time delay t_d as the time the front stays in a position whatever this position is. In Fig. 7(a), we have plotted the histogram of time delays. In the case $x=1.2$, the maximum of the t_d distribution is around 1. This means that the front stays locally in the same position (pixel) during $\Delta t=4$ ms. This corresponds precisely to the measured velocity of the front mean position $v_f=0.97$ pixels/Δt. For the composition Ti+1.4Si, the maximum is shifted to around 2 because the velocity is slower. The relay-race mechanism is more pronounced as reflected by the dispersion of the t_d distribution. The distribution becomes very broad for $x=1.5$, close to the combustion limit. Locally the front may stop for 20 ms, or even more.

The shape of the propagation front is far from being flat. The local deformations create holes and bumps which may be very pronounced, even visible, up to 1 mm. In Fig. 8, we have plotted the evolution of the front position $Y_f(i,t)$ for two contiguous columns j_1 and j_2 in the middle of the sample (with $j_2-j_1=10$ pixels). After ignition, the profile $Y_f(j_1,t)$ is ahead of $Y_f(j_2,t)$ for more than 100 Δt (0.4 s); but suddenly, at $t=120$ Δt, the local profile along j_1 crosses the other. The mutual crossing of propagation along contiguous columns may happen several times during one run. This is clear evidence of the local and instantaneous character of the strong deformations along the front during its evolution. We can get a more general picture of these properties by looking at the statistics of local instantaneous velocities [see Fig. 7(b)]. This quantity is essentially defined as the difference between two consecutive profiles $v(j,t)=Y_f(j,t+\delta t)-Y_f(j,t)$. If the front remains in the same position for a while, the velocity will vanish. If the front is distorted during the process, the velocity may become negative. For the composition Ti +1.5Si, the distribution is quite centered around zero with possible positive and negative velocities. In comparison, for the experiment with $x=1.2$, the distribution is dissymmetric in the positive range and its mean value corresponds to the mean velocity (1 pixel/s).

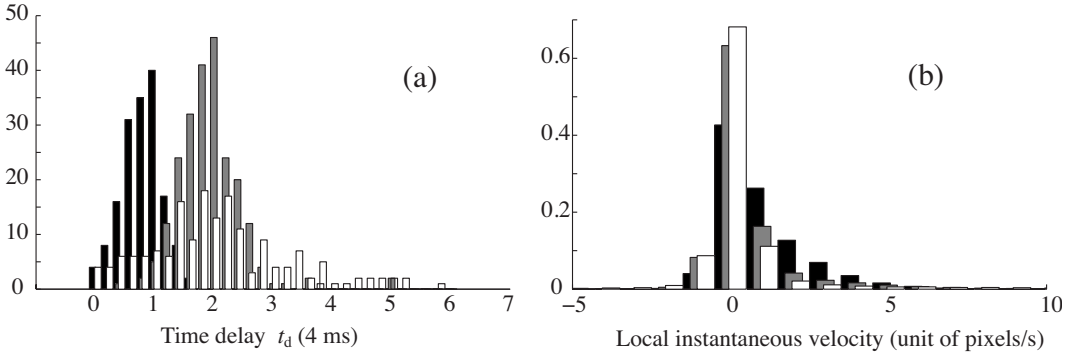

FIG. 7. (a) Histogram of time delays for different compositions: $x=1.2$ (black), $x=1.4$ (gray), and $x=1.5$ (white). (b) Histogram of local instantaneous velocities (same conditions). The velocity unit is pixels/s.

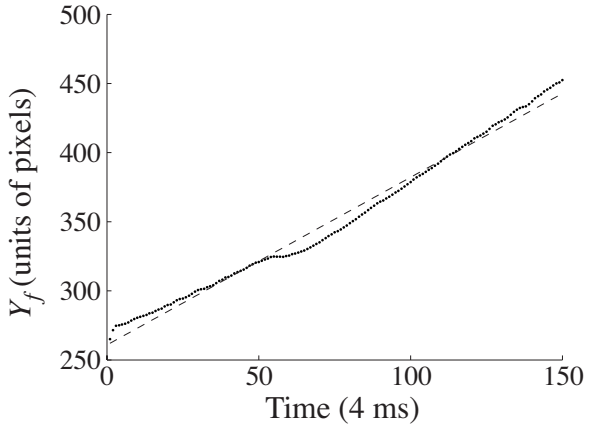

FIG. 9. Evolution of the mean front position $Y_{f,m}$ as a function of time in excess of titanium ($x=0.4$). We observe a deviation from the linear behavior represented by the dashed line.

C. Excess of titanium ($x<0.6$)

Let us first consider the case $x=0.4$. When plotting the mean position of the front $Y_{f,m}$ as a function of time, a strictly linear behavior is lost and two time scales are detectable as shown in Fig. 9. In a first stage, the front moves at 12 mm/s and then at speeds up to 16 mm/s. It indicates that we are probably crossing the boundary of steady-state behavior.

For smaller values of x, an instability regime clearly appears. Following a short transient period after initiation of combustion, the mean instantaneous position of the front $Y_{f,m}(t)$ starts to oscillate around a linearly increasing value y_ℓ. The Fourier transform of the signal $[Y_{f,m}(t)-y_\ell]$ demonstrates a well-defined frequency corresponding to an oscillation period of 50 ms as shown in Fig. 10.

The snapshots [Fig. 5(c)] show that the limit between burned products and fresh mixture is nearly flat. Nevertheless, the front structure is very different from those observed for a larger stoichiometric ratio [see Fig. 5(a)]. While the front is moving slowly downward, hot seats are propagating very fast in the lateral direction. After the passage of burning regions in the side surface of the sample, the front seems to stop before the appearance of a new set of hot spots in a subsequent layer. The combustion is pulsating: propagation steps alternate with static periods. If we had recorded this process at a common speed of 24 frames/s, we would observe a "one-dimensional" oscillating regime. The fact that ignition after depression does not occur simultaneously along the front becomes visible only at a high enough speed of video recording.

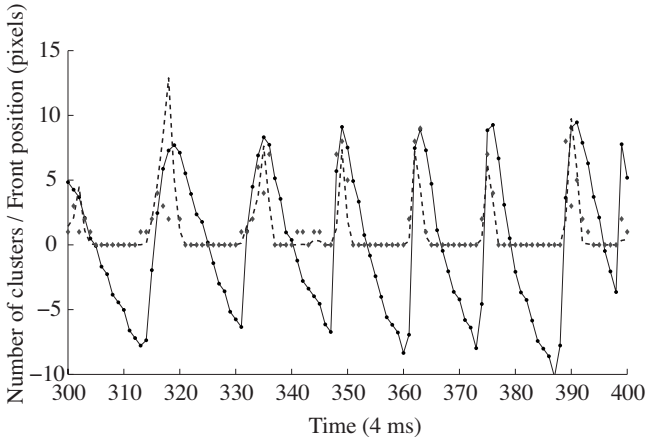

FIG. 11. Cluster dynamics as compared to position of the front: mean position of the front around the linear regression values $Y_{f,m}(t)-y_\ell$ (full line and dots), number of clusters n_{cl} (diamonds), and number of active sites n_{as} divided by 100 (dashed line).

It is interesting to characterize this process more quantitatively. The thickness of the burning layer is about 0.5 mm which is significantly larger than the typical size of the biggest particles (150 μm) of the system. A new spot appears every three or four frames ($\tau_1=50-60$ ms) while the preceding one has already reached the edge [see Fig. 5(c)]. The traveling time τ_2 of hot spots is significantly shorter (20–30 ms) than τ_1. The overall front stops during a latent period $\tau_2-\tau_1$. We can even further characterize the dynamical behavior of hot spots by using the tools developed in the framework of cluster size statistics in percolation theory. In our case, a hot spot is defined as a region of connected pixels whose brightness exceeds a predefined threshold value. The application of the Hoschen-Kopelman algorithm [31] on the images allows one to determine the number of clusters and their size. We have plotted in Fig. 11 the time evolution of the mean position $Y_{f,m}(t)-y_\ell$, the number of clusters n_{cl}, and the total number of active sites n_{as}. There is an evident cor-

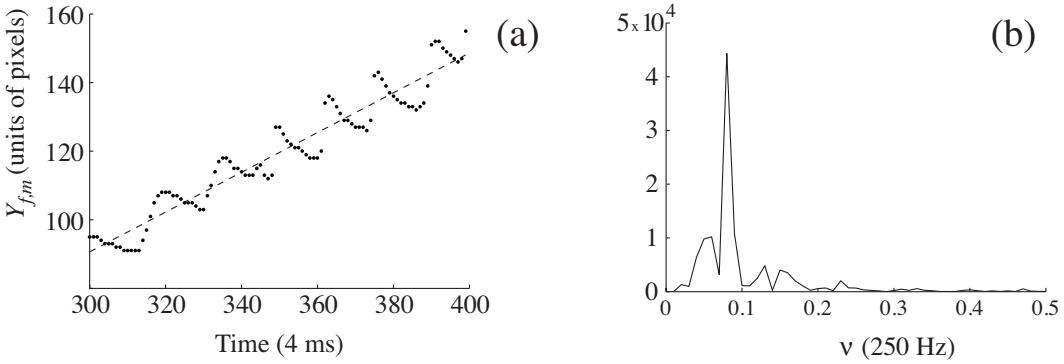

FIG. 10. (a) Evolution of the mean front position $Y_{f,m}$ as a function of time in excess of titanium ($x=0.324$). (b) Power spectrum of the position $[Y_{f,m}(t)-y_\ell]$ as a function of the frequency. The maximum at $\nu=0.08$ corresponds to a period of 0.05 s.

relation between the position evolution and the appearance of hot spots. Their absence corresponds to the slowing down of the front while the increase of the velocity arises just after the first birth. The individual clusters are countable and their total number never exceeds eight even if the bright sites cover a complete layer. Obviously, we do not have a spontaneous generation of local combustion centers but rather a collective behavior which affects the system layer after layer. All these facts suggest that the observed behavior appears as a consequence of the emerging instability.

V. DISCUSSION

The analysis based on the treatment of video frames reveals intrinsic features of the front propagation. In the composition range corresponding to an excess of Si, the roughness of the front is detectable with the naked eye. The complex structure of the front is not only the consequence of the heterogeneity of the support, but it is directly related to the spontaneous development of hot spots. These reactivity centers initiate locally the propagation while there is no combustion at all elsewhere. They are responsible for the relay-race mode of combustion which affects directly the propagation.

After its birth, a hot spot may grow by initiating the reaction in its neighboring regions. Then it spreads along the lateral direction of the front where the temperature is already high. Other spots may disappear without spreading. It appears thus that some hot spots are playing the role of precursor in the propagation. The hot spots production seems to have a purely random character. There is no systematic motion of hot spots along the front.

The support on which the reaction is taking place can be viewed as a random network of particles. Some of the connections between particles may be loose for the thermal transfer. As soon as a particle captures enough heat from one side, an exothermic reaction is initiated. If the heat transfer is inefficient with the other contiguous reactants particles, the temperature may increase and reach a value larger than the expected adiabatic temperature. The heat released by the reaction accumulates locally. This is the typical mechanism of explosion: the heat transfer ceases to compensate the heat production. Appropriate modeling such as the cellular model has been developed to account for these aspects [32,33].

Since the discovery of a new combustion regime associated with the heterogeneity of the reactive medium, most of the studies have been dedicated to study the influence of the support on the scintillating phenomena. The effects of particle size and porosity have been systematically investigated [20]. The correlation between the microscopic properties and the propagation characteristics has been demonstrated experimentally. In this work, we have developed a different type of analysis. All the experiments were carried out on samples that have the same microstructure. The only parameter that has been changed is the combustion temperature T_C which is typically a macroscopic control parameter. By changing its value, one expects to observe the development of instabilities before reaching the combustion limit. In excess of Si ($x>0.6$), no oscillation phenomenon was observed. When T_C decreases, the front moves more slowly until it stops completely and there is no combustion at all. Nevertheless, the dynamical behavior is changing since the relay-race mechanism becomes more pronounced. The periods of time during which the front does not propagate locally (time delays) become more and more long as T_C reaches the combustion limit. This feature looks very similar to the critical slowing down that appears close to a bifurcation point. It corroborates the picture of the system we have proposed: a reactive network of loosely connected particles where ultralocalized explosions occur. As the distance from the transition limit diminishes, we observe that the time delay increases notably which means that the ignition time in each "reactor" becomes larger. This situation supports the sensitivity of the system to any perturbation and enhances the random and spontaneous development of hot spots [9].

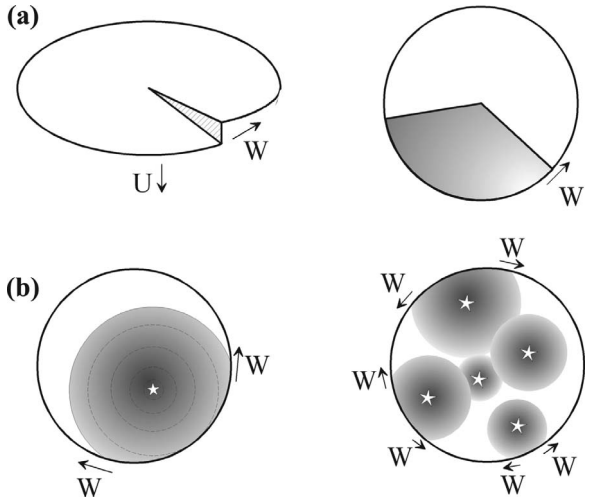

FIG. 12. (a) Schematic illustration of the spin combustion regime. The spin wave is propagating with a constant velocity along the helical trajectory on the side surface of the sample. Egress of the front on the end side of the sample looks like a growing sector of a circle whose radius is precisely the radius of the sample and the angle increases linearly with time. (b) Possible mechanism of the *quasispin combustion regime*: local ignition and radial growing of the reactive fronts. When the very reactive external layer of the front crosses the side surface of the sample, hot spots become visible by the observer. Their motion on the side surface results from the growing of the surface front.

In the Ti-rich concentration region, in the vicinity of the combustion limit ($x\approx 0.3$), we observe a radically different behavior which shows some of the characteristics of a spin-combustion regime: oscillations of the position due to the alternation of static and fast burning periods as well as the rapid circular motion of hot seats. As we have shown in the previous section, the front position oscillation is clearly associated with the bright spots appearing on the lateral side of the sample. The understanding of the mechanism responsible for hot seats generation is challenging. To what extent do we recover the behavior predicted by the macroscopic approach in which the spin combustion arises either from spiral motion of steplike disturbance of the combustion front [26] (see Fig. 12) or as a spiral-helix motion of localized hot spots moving with a constant rotary velocity on the side surface?

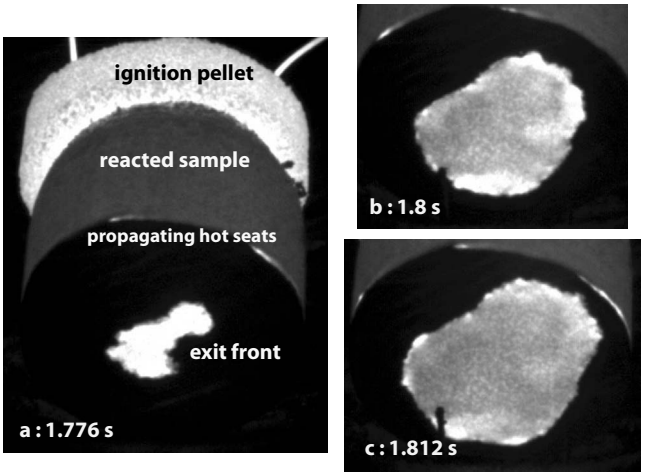

FIG. 13. In this experiment, the sample has been tilted to visualize the egress of the combustion wave on the end surface. In the left image, we see what it looks like: the tungsten wire and the ignition pellet, the reacted sample after the passage of the front, and the exit end surface ($d=13$ mm).

To figure out what happens inside the sample during the experiment is a tricky problem. This is nevertheless the only way to discover the characteristics of the reactive front. For this purpose, we have titled the sample in the reaction chamber and focused the camera on the end surface (Fig. 13). In this way, we were able to look at the formation of the exit of the combustion wave. Results of this experiment show a radial growing distorted circle on the end-side surface and multiple hot seats of different sizes propagating on the side surface of the sample. We clearly observe that the combustion arises due to a localized ignition. The reaction probably starts within a thin preheated disk of the reaction mixture, next to hot solid products of combustion. While the exit front is appearing, hot seats continue to move on the lateral side. Combustion spots are observable together on the sample side and at the border of the active front. A plausible scenario of this *quasispin regime* is the following [see Fig. 12(b) and [34]]:

(1) local random ignition in preheated layers;

(2) radial expansion of the front; and

(3) high activities on the external layer which persist until crossing the side surface of the sample.

In this combustion regime, the front surface becomes unstable and shows a nonuniform shape with moving external combustion seats. Although we recover some features of the complexity of the combustion surface predicted by Ivleva and Merzhanov in their simulations of three-dimensional cylindrical systems [13,28], our experimental results suggest nevertheless a slightly different interpretation.

VI. CONCLUDING REMARKS

In this paper, we have presented an experimental investigation of the nonlinear behavior of self-propagating high-temperature synthesis waves in the full range of combustibility. *In situ* imaging analysis allows one to study the dynamical and structural properties of the fronts and to detect the complexity of the combustion patterns. A quasispin regime results from the instability of the process near the metal-rich concentration limit while a pronounced scintillating regime occurs near the nonmetal-rich limit.

We have shown that the combustion temperature T_C as compared to the melting temperature of the reactants plays a significant role in the emergence of instabilities. The quasispin regime is clearly associated with a solid combustion, while relay-race combustion is predominant for a liquid-solid system. Moreover, the physical state of the reactants has certainly a strong influence on the reactive mechanisms at the level of individual grains. Preliminary experimental results show the formation of multilayers of intermediate compounds. It would be interesting to investigate the role of the temperature pulse and of the front dynamical behavior on the observed microstructures [35].

Our study demonstrates that the sensitivity of such reactive fronts becomes especially striking in the close vicinity of instabilities, like, for instance, the enhancement of time delays in the relay-race regime near the combustion limit. It appears thus that the modeling of these systems should not be restricted to the usual macroscopic description but should include the essential features of the intrinsic microheterogeneity as can be done in discrete models.

ACKNOWLEDGMENTS

This work was supported by the Joint French-Russian Program for Scientific Cooperation (Grants No. PICS 346 SC-CNRS and No. RFBR 06-03-22000). One of the authors (A.S.R.) was supported by CNRS during his visit to the Institut Carnot de Bourgogne.

[1] G. Nicolis and C. Nicolis, *Foundations of Complex systems: Nonlinear Dynamics, Statistical Physics, Information and Prediction* (World Scientific, Singapore, 2007).

[2] G. Nicolis, *Introduction of Nonlinear Science* (Cambridge Univ. Press, Cambridge, England, 1995).

[3] I. R. Epstein and J. A. Pojman, *An Introduction of Nonlinear Chemical Dynamics: Oscillations, Waves, Patterns and Chaos* (Oxford University Press, New York, 1998).

[4] D. K. Kondepudi, *Introduction to Modern Thermodynamics* (Wiley, New York, 2008).

[5] F. Baras and M. Malek Mansour, Adv. Chem. Phys. **100**, 393 (1997).

[6] Y. De Decker, F. Baras, G. Nicolis, and N. Kruse, J. Chem. Phys. **117**, 10244 (2002).

[7] Yu. Suchorski, J. Beben, E. W. James, J. W. Evans, and R. Imbihl, Phys. Rev. Lett. **82**, 1907 (1999); Yu. Suchorski, J. Beben, R. Imbihl, E. W. James, Da-Jiang Liu, and J. W. Evans, Phys. Rev. B **63**, 165417 (2001).

[8] F. Baras, G. Nicolis, M. Malek Mansour, and J. W. Turner, J. Stat. Phys. **32**, 1 (1983).
[9] G. Nicolis and F. Baras, J. Stat. Phys. **48**, 1071 (1987).
[10] A. Lemarchand, R. I. Ben Aïm, and G. Nicolis, Chem. Phys. Lett. **162**, 92 (1989).
[11] B. J. Matkowsky and G. I. Shivashinsky, SIAM J. Appl. Math. **35**, 465 (1978).
[12] A. G. Merzhanov and B. I. Khaikin, Prog. Energy Combust. Sci. **14**, 1 (1988).
[13] T. P. Ivleva and A. G. Merzhanov, Phys. Rev. E **64**, 036218 (2001).
[14] A. G. Merzhanov, Russ. Chem. Rev. **72**, 289 (2003).
[15] A. G. Merzhanov, J. Mater. Chem. **14**, 1779 (2004).
[16] A. S. Rogachev, V. A. Shugaev, C. R. Kachelmyer, and A. Varma, Chem. Eng. Sci. **49**, 4949 (1994).
[17] A. S. Mukasyan, S. Hwang, A. E. Sytchev, A. S. Rogachev, A. G. Merzhanov, and A. Varma, Combust. Sci. Technol. **115**, 335 (1996).
[18] A. Varma, A. S. Rogachev, A. S. Mukasyan, and S. Hwang, Proc. Natl. Acad. Sci. U.S.A. **95**, 11053 (1998).
[19] A. S. Mukasyan, A. S. Rogachev, and A. Varma, Chem. Eng. Sci. **54**, 3357 (1999).
[20] A. S. Mukasyan, A. S. Rogachev, M. Mercedes, and A. Varma, Chem. Eng. Sci. **59**, 5099 (2004).
[21] A. G. Merzhanov, Combust. Flame **13**, 143 (1969).
[22] D. A. Frank-Kamenetskii, *Diffusion and Heat Transfer in Chemical Kinetics* (Plenum Press, New York, 1969).
[23] A. S. Rogachev, Int. J. Self-Propag. High-Temp. Synth. **6**, 215 (1997).
[24] G. M. Machviladze and B. V. Novozilov, Prikl. Mekh. Tekh. Fiz. **5**, 51 (1971).
[25] K. G. Shkadinskii, B. I. Khaikin, and A. G. Merzhanov, Combust., Explos. Shock Waves **7**, 15 (1971).
[26] Yu. M. Maksimov, A. G. Merzhanov, A. T. Pak, and M. N. Kuchkin, Combust., Explos. Shock Waves **17**, 393 (1981).
[27] T. P. Ivleva and A. G. Merzhanov, Dokl. Phys. **45**, 136 (2000).
[28] T. P. Ivleva and A. G. Merzhanov, Chaos **13**, 80 (2003).
[29] Ya. B. Zeldovich, Zh. Eksp. Teor. Fiz. **11**, 159 (1941) (in Russian).
[30] D. B. Spalding, Proc. R. Soc. London, Ser. A **240**, 83 (1957).
[31] J. Hoshen and R. Kopelman, Phys. Rev. B **14**, 3438 (1976); A. Al-Futaisi and T. W. Patzek, Physica A **321**, 665 (2003).
[32] A. S. Rogachev, Combust., Explos. Shock Waves **39**, 150 (2003).
[33] A. S. Rogachev and F. Baras, Int. J. Self-Propag. High-Temp. Synth. **16**, 141 (2007).
[34] F. Baras and A. S. Rogachev, Combust. Flame (to be published).
[35] F. Baras and D. Kondepudi, J. Phys. Chem. B **111**, 6457 (2007).
[36] A mixture Ti+xSi characterized by the stoichiometric coefficient x is made of a moles of Ti and xa moles of Si. For instance, to prepare the well-defined intermetallic compound Ti_5Si_3, we take $5a$ moles of Ti and $3a$ moles of Si which corresponds to $x=0.6$.